FEBS Letters 580 (2006) 5885–5893

A novel analytical method for in vivo phosphate tracking

Hong Gu[a,b,1,2], Sylvie Lalonde[a,1], Sakiko Okumoto[a,1], Loren L. Looger[a], Anne Marie Scharff-Poulsen[b], Arthur R. Grossman[a], Jens Kossmann[b,c], Iver Jakobsen[b], Wolf B. Frommer[a,*]

[a] *Carnegie Institution, Department of Plant Biology, 260 Panama Street, Stanford, CA 94305, USA*
[b] *Biosystems Department, Risø National Laboratory, Roskilde 4000, Denmark*
[c] *Institute for Plant Biotechnology, Stellenbosch University, Private Bag X1, Matieland 7602, South Africa*

Received 10 July 2006; revised 14 September 2006; accepted 22 September 2006

Available online 2 October 2006

Edited by Michael R. Bubb

Abstract **Genetically-encoded fluorescence resonance energy transfer (FRET) sensors for phosphate (P_i) (FLIPPi) were engineered by fusing a predicted *Synechococcus* phosphate-binding protein (PiBP) to eCFP and Venus. Purified fluorescent indicator protein for inorganic phosphate (FLIPPi), in which the fluorophores are attached to the same PiBP lobe, shows P_i-dependent increases in FRET efficiency. FLIPPi affinity mutants cover P_i changes over eight orders of magnitude. COS-7 cells co-expressing a low-affinity FLIPPi and a Na^+/P_i co-transporter exhibited FRET changes when perfused with 100 μM P_i, demonstrating concentrative P_i uptake by PiT2. FLIPPi sensors are suitable for real-time monitoring of P_i metabolism in living cells, providing a new tool for fluxomics, analysis of pathophysiology or changes of P_i during cell migration.**

Keywords: Fluorescence energy transfer; Phosphate starvation; Biosensor; *Synechococcus*

1. Introduction

Phosphate (P_i) is an essential macronutrient for all living organisms. It serves central biological functions as part of nucleic acids, phospholipids and ATP, as a metabolite involved in energy transfer, as a component of signal transduction cascades, and in the regulation of enzymes and metabolic processes. Adenosine triphosphate (ATP) is the dominant 'energy currency' in the cell; the hydrolysis of ATP to adenosine diphosphate (ADP) plus P_i releases energy that fuels most energy-requiring processes in the cell. Indeed, ATP is required for phosphorylation of glucose, which enables the glucose to enter the glycolytic pathway. Moreover P_i is essential for the skeleton, with 85% of the total body P_i incorporated into the bone. Therefore, P_i is a critical metabolite, and subtle concentration changes of this molecule can profoundly alter cellular growth and metabolism. Cellular uptake is mediated by concentrative P_i transporters, which in mammalian cells use the proton and sodium gradients [1]. Since P_i and phosphorylated compounds are present in all cellular compartments, and since their concentrations can differ significantly between cells in a specific tissue type, and between the compartments within a cell [2], it is important to develop tools that permit quantitative determination of changes in the P_i concentration in living cells with subcellular resolution. ^{31}P NMR can only be used to determine subcellular distribution of P_i within tissue samples in cases, where pH differs between compartments, and P_i concentrations are in the millimolar range [2]. A high-sensitivity methodology that would allow for dynamic analysis of P_i in subcellular compartments is still lacking.

The uptake of P_i into Gram-negative bacteria, such as *Escherichia coli* and *Salmonella*, is mediated by the combined action of an outer membrane porin, a periplasmic P_i-specific binding protein (PiBP), and an inner membrane ABC transporter. PiBP binds both monobasic ($H_2PO_4^-$) and dibasic (HPO_4^{2-}) phosphate [3] with an overall apparent K_d of 0.8 μM [4]; the dissociation rate constant was determined to be 21 s^{-1} at neutral pH and low ionic strength [5]. PiBP consists of two globular domains connected by a flexible hinge [6]. In the absence of P_i, PiBP globular domains are separated, exposing a cleft that is accessible to soluble metabolites. Binding of PiBP to P_i induces a conformational change in which the two globular domains of the protein come closer together, solvent is excluded from the binding pocket and hydrogen bonds form between the amino acids of PiBP and bound P_i [7].

PiBP from *E. coli* functions as an in vitro P_i sensor when coupled to the fluorophore N-[2-(1-maleimidyl)ethyl]-7-(diethylamino)coumarin-3-carboxamide (MDCC) [8,9]; *E. coli* PiBP was independently shown to signal P_i binding via any of six small molecule dyes [10]. However, such dyes are difficult to introduce into living cells, cannot be easily localized to subcellular compartments, and are likely toxic to cells. The availability of genetically-encoded FRET sensors for P_i would enable systematic screening of mutant collections for factors that control P_i homeostasis, or of chemical libraries to identify novel drugs.

Fluorescence resonance energy transfer (FRET) between chromatic variants of the green fluorescent protein (GFP) can be exploited to monitor conformational changes in

*Corresponding author. Fax: +1 6503256857.
E-mail address: wfrommer@stanford.edu (W.B. Frommer).

[1] These authors contributed equally.
[2] Present address: Plant Physiology and Anatomy Laboratory, The Royal Veterinary and Agricultural University, Thorvaldsensvej 40, DK-1871 Frederiksberg C, Denmark.

Abbreviations: FLIPPi, fluorescent indicator protein for inorganic phosphate; FRET, fluorescence resonance energy transfer; FP, fluorescent protein

0014-5793/$32.00
doi:10.1016/j.febslet.2006.09.048

proteins [11,12]. The allosteric coupling between ligand binding and FRET can be used to quantitatively measure analyte levels; indeed, nanosensors for sugars (e.g. maltose, ribose, and glucose [13–16]) and amino acids (e.g. glutamate [17]) have been created by fusing a bacterial periplasmic-binding protein specific for a given ligand to FRET donor and acceptor fluorophores. These ratiometric nanosensors were expressed in live cells and used for in vivo analysis of metabolite concentrations in the cytosol, in the nucleus, inside the ER lumen and at the cell surface [13–15,17–19].

The *Synechococcus* PiBP, by homology with the *E. coli* PiBP [3,7], is predicted to be a type II PBP, with both termini on the same protein lobe. It has been previously shown that such proteins, when fused to FRET donor and acceptor fluorophores, can make good sensors (as in the case of the *E. coli* glutamate/aspartate-binding protein [17,20]), indicating that other subtle effects (dipole orientation changes, surface interactions between PiBP and fluorophores) in addition to changes in distance between the donor and acceptor fluorophores contribute to the FRET transfer efficiency.

We tested several PiBPs linearly fused with eCFP and Venus (an eYFP variant with reduced pH and chloride sensitivity [21]), in search of a sensor for which P_i elicits a significant change in FRET. A suitable sensor was created from a *Synechococcus* protein predicted by sequence homology to be a P_i-binding protein; the response of the sensor was modest, saturable, and consistent with a single P_i-binding site. The sensor was optimized by site-directed mutagenesis of the binding protein–chromophore linkers and the P_i-binding pocket to improve the signal change, and to create a family of sensors with variant affinities.

When FLIPPi (fluorescent indicator protein for inorganic phosphate) with a K_d of 30 mM was expressed in P_i-starved Chinese hamster ovary (CHO) cells, it responded to extracellular P_i with a reduced Venus/eCFP fluorescence emission intensity ratio. A FLIPPi variant with a K_d of 5 μM did not respond to P_i perfusion, consistent with the hypothesis that the intracellular concentration of P_i is outside of the dynamic range of this higher-affinity sensor. Additionally, the sensor reliably detected changes in external P_i availability of unstarved COS-7 cells that were over-expressing a Na^+/P_i cotransporter. This new family of FLIPPi sensors can be used to monitor P_i levels over a wide dynamic range that encompass those levels that typically occur in living cells.

2. Materials and methods

2.1. FLIPPi constructs and plasmids

A truncated PiBP (*Synechococcus* strain A; ORF01723), encoding the predicted mature protein without periplasmic leader sequence, was amplified by PCR from genomic DNA of the thermophilic cyanobacterium [22] using the primers 5′-ATTGGTACCGTAGGATTTCTAACAGCG-3′ and 5′-ATAGGTACCGTTAACGGTGATGGAATC-3′. The PCR fragment was cloned into the *Kpn*I site of FLIPmal-25μ [13] in pRSET-B (Invitrogen, USA), exchanging the sequence encoding the maltose-binding protein with that of PiBP. The resulting plasmid was named pRSET-FLIPPi-840n. To improve the fluorophore maturation efficiency and the pH- and chloride-tolerance of the sensor, the sequence of eYFP in pRSET-FLIPPi-840n was replaced with that of the YFP variant Venus [21], and the composite linkers were shortened by site-directed mutagenesis to yield FLIPPi-260n. Affinity mutants of FLIPPi were created by site-directed mutagenesis [41], generating the T22A, S52A, G162A and T163A variant sensor proteins. These pRSET-FLIPPi constructs were introduced into *E. coli* BL21(DE3)Gold (Stratagene, USA) by electroporation, and the expressed proteins were extracted and purified as described [13]. For expression in the cytosol of CHO cells, DNA fragments containing FLIPPi-5μ and FLIPPi-30m sequences were excised from pRSET-FLIPPi-5μ and pRSET-FLIPPi-30m, respectively, with *Bam*HI/*Hind*III and cloned into pCDNA3.1 (Invitrogen, USA). For the co-expression of FLIPPi-30m and the human Na^+/Pi transporter PiT2, an *EcoRV* site was introduced at the 3′- end of the eGFP sequence in pCMS-eGFP (Clontech, USA), and the eGFP sequence was replaced by the *Bam*HI–*Pme*I fragment from pcDNA3.1-FLIPPi-30m. The resulting plasmid was named pCMS-FLIPPi-30m. pcDNA-PiT2, which carries the VSV-tagged human PiT2 transporter, was kindly provided by Dr. Heard (Institut Pasteur, France). pcDNA-PiT2 was digested with *Hind*III, blunted, and the PiT2 sequence was excised with *Not*I and cloned into *Xho*I (blunt-ended)/*Not*I sites in pCMS-FLIPPi-30m.

2.2. In vitro characterization of FLIPPi

Emission spectra and ligand titration curves were obtained using a monochromator microplate reader (Safire, Tecan, Austria, excitation 433/12 nm; emission 485/12 and 528/12 nm; gain 70). Enzymatic P_i-depletion of buffers was achieved by overnight dialysis against 1 U nucleoside phosphorylase and 1 mM inosine (Sigma, USA). All assays were performed in 20 mM Tris–HCl buffer, pH 7.0. The K_d of each FLIPPi sensor was determined by fitting ligand titration curves to a single-site binding isotherm: $S = (r - r_{apo})/(r_{sat} - r_{apo}) = [L]/(K_d + [L])$, where S is saturation; $[L]$, ligand concentration; r, ratio; r_{apo}, ratio in the absence of ligand; and r_{sat}, ratio at saturation with ligand. Measurements were performed with at least three independent protein extracts.

2.3. Cell culture and transfection

Chinese hamster CHO cells were grown in minimum essential MEM-α medium supplemented with 10% fetal bovine serum (Gibco). Cells were cultured at 37 °C and 5% CO_2. For imaging, the cells were cultured in eight-well tissue culture glass slides (BD Falcon). The efficiency of transfection, performed using Lipofectamine 2000 (Invitrogen, USA) and determined by counting fluorescent cells, was at least 30%. Cell starvation was started 16 h prior to the experiment by replacement of MEM-α medium with modified Tyrode's saline solution containing 100 mM MOPS, 2.5 mM KCl, 25 mM HEPES, 30 mM glucose, 2 mM $CaCl_2$ and 2 mM $MgCl_2$. COS-7 cells were grown in DMEM medium supplemented with 10% FBS (Difco, USA) on poly-D-lysine (Sigma) coated cover slips.

2.4. Imaging of cell cultures

CHO and COS-7 cells were analyzed for FRET 24–48 h after transfection, using an inverted epifluorescence microscope (DM IRE2, Leica, Germany) with a cooled CoolSnap HQ digital camera (Photometrics, USA) and a 63× water immersion lens (HCX PL APO, Leica, Germany). Dual emission intensity ratios were simultaneously recorded using a DualView with an OI-5-EM filter set (Optical Insights, USA) and Metafluor 6.3 software (Molecular Devices, USA). Depending on expression level, the exposure times varied between 0.5 and 2.5 s. Unless stated otherwise, CHO cells were perfused with P_i-free modified Tyrode's saline solution at a flow rate of 1.8 ml/min in a chamber with a total volume of <0.6 ml. For each imaging experiment, at least three independent repetitions were performed. COS-7 cells were perfused with P_i-free Tyrode's saline solution. Confocal analysis was performed as described [38].

3. Results

3.1. Identification of a PiPB suitable for sensor design

The PiBP protein from *E. coli* allosterically signals P_i binding in conjunction with a variety of small molecule dyes [10]; therefore, this protein scaffold was selected for conversion to a FRET sensor. Fusion constructs were expressed in *E. coli*, protein was isolated by His affinity chromatography and the FRET change was measured in a buffer solution enzymatically

depleted of P_i, to which P_i was added at the desired concentration. P_i levels above 5 mM led to significant fluorescence quenching (data not shown).

The PiBP sensor initially constructed was found to have a high FRET efficiency, but exhibited no P_i-dependent change (data not shown). We therefore sought to identify additional P_i-binding domains that could be used to construct sensor that would respond to the P_i concentration. We constructed a phylogenetic tree of putative P_i-binding proteins from several bacterial species (Supplementary Fig. 1) and used this tree to select representatives from evolutionarily divergent subclades, reasoning that this strategy might increase our sampling of potential dipole–dipole relative orientations of the donor and acceptor fluorophores. The sensors generated from PiBP genes from *Pyrococcus furiosus* and *Sulfolobus solfataricus* also failed to show a significant FRET change, but one constructed using a PiBP homologue from the thermophilic *Synechococcus* strain OS-A [22] did exhibit a phosphate-dependent FRET increase; this sensor was designated FLIPPi-WT. The affinity of this sensor for P_i was 840 nM (with a Hill coefficient of 1.03), consistent with the 800 nM K_d reported for the *E. coli* PiBP [4]. The ratio change observed for FLIPPi-WT was 0.14 (6% change; Fig. 1a). It is thus apparently possible to obtain a functional FRET sensor even for proteins in which the fluorophore attachment is adjacent on the same lobe.

3.2. Mutants with altered P_i affinity and improved signal change

Previous studies had shown that shortening the flexible domains linking the binding protein with the fluorophores could improve the allosteric coupling and thus the FRET signal change [20]; a total of 18 amino acids were thus shortened from the sensor sequence: 9 from the C-terminus of the eCFP, 1 from the N-terminus of Venus, and 4 from each binding protein–fluorophore linker (Fig. 1b). Titration of this modified protein (designated FLIPPi-260n) gave an increase in eCFP emission and a decrease in Venus emission, resulting in a P_i-dependent decrease in FRET. The binding constant for P_i was determined to be 260 nM, with a maximum ratio change of −0.13 (7%; Fig. 1c). Linker deletion has thus reversed the sign of the FRET ratio change without altering the magnitude; the affinity has also been slightly increased.

As a basis for further signal enhancement and for designing affinity mutants, the PiBP sequences of *Synechococcus* sp. and *E. coli* were aligned (identity 37%) and a homology model was generated with 3D-JIGSAW [23] (*E. coli* PiBP: Protein Data Bank structural identifier 1a40) (Fig. 2). To expand the dynamic range of the P_i sensor family, site-directed mutagenesis was used to decrease the P_i-binding affinity. The P_i present in the binding pocket of *E. coli* PiBP is held in place by strong hydrogen bonds [24]; the structural alignment of the binding pockets of the *E. coli* structure and the *Synechococcus* model shows that the interacting side-chains are completely conserved, except for the conservative substitution of Asp56 in the *E. coli* protein to Glu70 in the *Synechococcus* protein (Fig. 2c). Five residues of FLIPPi-260n were selected for site-directed mutagenesis, generating a set of sensors with a broad range of P_i-binding affinities (Fig. 1d and Table 1). All five affinity mutants showed a greatly improved FRET change upon P_i binding (8–10-fold), predominantly through an increase of the apo FRET efficiency. This is consistent with either or both of two scenarios: (i) residual P_i is bound to the high-affinity sensors and artificially depresses the signal change, or (ii) the FRET efficiency of the apo and/or ligand-bound states of the sensor is perturbed by an alteration of

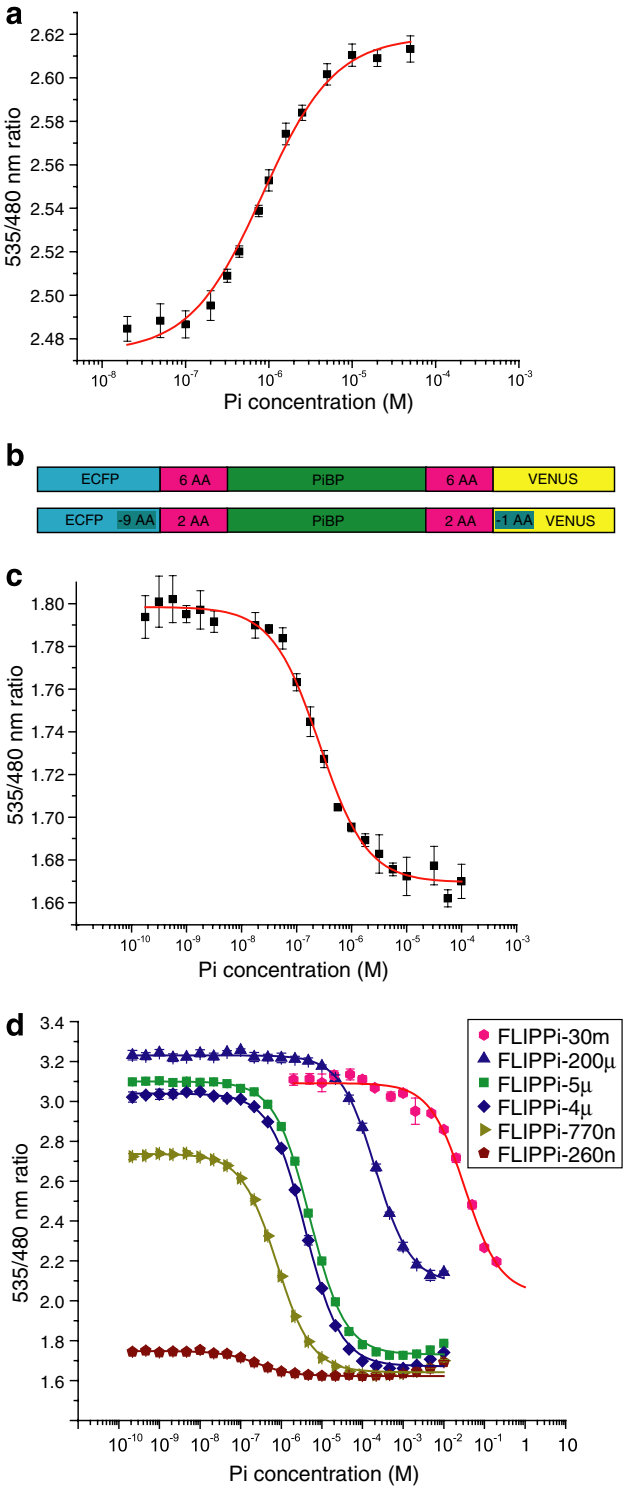

Fig. 1. (a) In vitro ligand-dependent FRET changes of FLIPPi-WT purified nanosensors. Non-linear regression best fit and error bars are shown. (b) FLIPPi-WT construct (above); FLIPPi-260n construct (below; nine amino acids were deleted from the C-terminus of the eCFP, one from the N-terminus of Venus, and four from each binding protein-fluorophore linker). (c) and (d) In vitro ligand-dependent FRET changes of FLIPPi-260n (c) and affinity mutants of the FLIPPi-260n construct (d; Table 1).

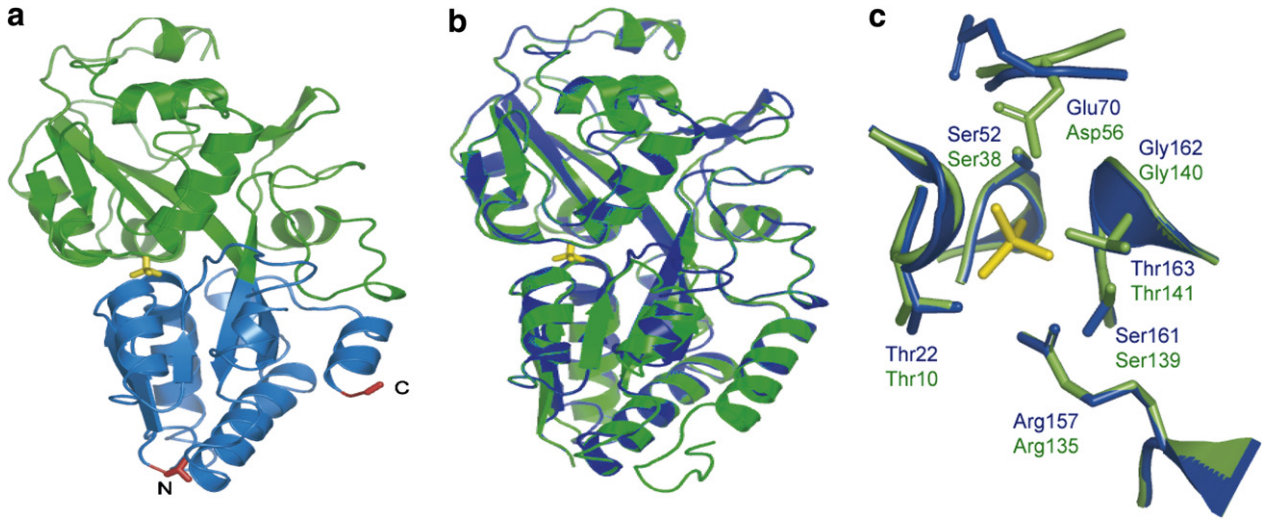

Fig. 2. The predicted structure of PiBP in alignment with the *E. coli* PiBP (PDB 1a40). (a) *Synechococcus* PiBP structural model, predicted by 3D-JIGSAW. Phosphate is in yellow, and the N- and C-termini in red. Terminal lobe, blue; other lobe, green. (b) Alignment of the model (blue) with the crystal structure of *E. coli* (green). (c) Alignment of binding sites. The only sequence difference is Glu70 in FLIPPi and Asp56 in *E. coli*. The *Synechococcus* structure has likely been poorly modeled in the region of Glu70 and Ser161 (phosphate was not present in the 3D-JIGSAW modeling step). Green: *E. coli*; blue: FLIPPi; yellow: phosphate.

Table 1
FLIPPi affinity mutants

Sensor	Sequence	K_d (M)[a]	ΔR_{max}[a,b]	Hill coefficient	Dynamic range[c]
FLIPPi-260n	Wild-type	2.6×10^{-7}	−0.13	1.03	25–1200 nM
FLIPPi-770n	S161A	7.7×10^{-7}	−1.07	1.03	80–5600 nM
FLIPPi-4μ	T163A	3.9×10^{-6}	−1.34	1.02	0.4–25 μM
FLIPPi-5μ	S52A	5.1×10^{-6}	−1.33	1.03	0.5–34 μM
FLIPPi-200μ	G162A	2.1×10^{-4}	−1.13	1.00	25–1600 μM
FLIPPi-30m	T22A	3.3×10^{-2}	−1.03	1.03	3–170 mM

Binding constants determined in vitro.
[a] R^2 for the fit exceeded 0.98 in all analyses.
[b] ΔR_{max}, in vitro maximum change in ratio between ligand-free and ligand-saturated sensor.
[c] Range between 10% and 90% saturation of the sensor (the effective quantification range).

the precise open and closed state forms, which could impact relative dipole orientations and thus FRET efficiency [20]. The mutants were designated FLIPPi-770n, FLIPPi-4μ, FLIPPi-5μ, FLIPPi-200μ, and FLIPPi-30m, according to their P_i-binding affinity. The computed Hill coefficients of all PiBPs are very close to 1, consistent with a single P_i-binding site [4]. The improved dynamic ranges of the individual sensors (due to their greater signal-to-noise ratios) in conjunction with the distribution of their equilibrium binding constants, creates a wide composite dynamic range of the set of all six sensors, covering 30 nM–150 mM, except for the interval of 1.5–3 mM (Fig. 1d and Table 1). To determine the substrate specificity and pH sensitivity of the sensor in the physiological range, the pH dependence of phosphate binding as well as the response to sulfate and nitrate was tested for FLIPPi-5μ (Fig. 3). FLIPPi-5μ did not respond to nitrate or sulfate, moreover, the binding isotherms for phosphate were very similar between pH 6.8 and 7.6. Since the K_d did not shift significantly, despite the significant relative change in the relative amounts of HPO_4^{2-} and $H_2PO_4^-$ (pK_a 7.2), the sensor appears independent of pH changes in this range due to similar recognition of both forms.

Previous analyses have suggested that intracellular P_i concentrations are in the range of 1–10 mM [2,25–27], thus the single sensor FLIPPi-30m (dynamic range 3–170 mM) or the combination of FLIPPi-30m and FLIPPi-200μ offer the best starting points for monitoring in vivo P_i concentrations.

3.3. Sensor response in P_i-starved CHO cells

"Cytosolic" P_i levels (including the endoplasmic reticulum and all cytoplasmic organelles) have been estimated at approximately 6 mM in both plant and animal cells [25,27]. Thus, the FLIPPi-30m sensor seems well suited to monitor physiologically-relevant P_i concentrations (in contrast to the other sensors, which should be fully-saturated). CHO cells were independently transfected with either the FLIPPi-30m "working" or FLIPPi-200μ and FLIPPi-5μ "control" sensors. The chimeric protein is distributed evenly within the cytosol and is excluded from vesicular bodies and the nucleus (Fig. 4a). Initial experiments with resting CHO cells showed no FRET change for either sensor upon perfusion with up to 10 mM P_i, suggesting limiting transport rates. P_i deprivation is known to regulate Na^+/P_i transporter activity [1]. Therefore, CHO cells were grown overnight after transfection and P_i-starved

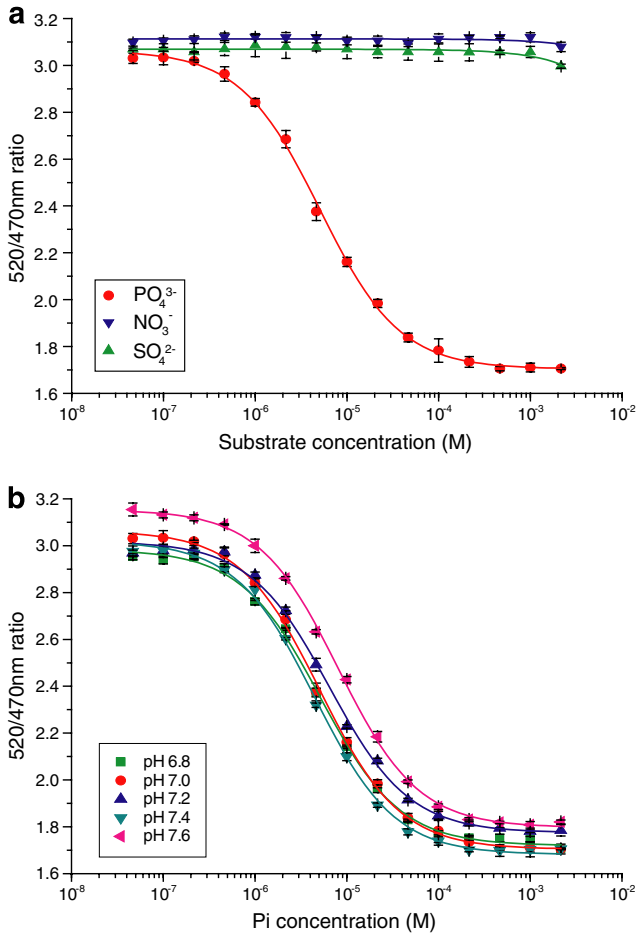

Fig. 3. Specificity and pH sensitivity of FLIPPi-5μ. (a) Selectivity of FLIPPi-5μ for phosphate over nitrate and sulfate. Solid lines were plotted by curve fitting. (b) Phosphate binding of FLIPPi-5μ was tested in 20 mM Tris buffers adjusted to pH 6.8, 7.0, 7.2, 7.4 and 7.6, then titrated with phosphate solutions of the same respective pH. Statistical analysis (ANOVA) showed no significant difference regarding the maximal ratio change between pH 6.8 and 7.4.

for 16 h by replacing P_i-replete growth medium with modified Tyrode's saline solution lacking P_i, before making the measurements. Cells expressing FLIPPi-30m were perfused with increasing concentrations of external P_i, and changes in the fluorescence peak emission ratio were monitored (Fig. 4b). After a stable YFP/CFP emission intensity ratio was attained at each P_i concentration, P_i was removed by perfusion with P_i-free solution, returning the sensor fairly rapidly to baseline emission. FLIPPi-5μ did not show a signal change upon perfusion with even a high concentration of P_i (Fig. 4c). Similar results were obtained for FLIPPi-200μ (data not shown). Starved cells expressing FLIPPi-30m responded to solutions containing 50 μM and 100 μM P_i; the ratio change was significantly higher at 100 μM external P_i (Fig. 4b). Under the conditions used (118 mM NaCl, pH 7.3), the endogenous Na^+/P_i cotransporters should theoretically be able to concentrate P_i inside the cells up to 100-fold, consistent with the increase observed using the FLIPPi-30m sensor [1]. Cells were highly sensitive after starvation, however, and either lost fluorescence or detached from the slide during the experiment. Thus, the responses were not robust enough for a more detailed analysis of flux.

3.4. Co-expression of a Na^+/Pi transporter and the FRET sensor in COS-7 cells

Similarly, COS-7 cells expressing the FLIPPi-30m sensor also did not reproducibly respond to perfused P_i (data not shown). It is known that phosphate transport activities are down-regulated by external P_i [28,29]. As an alternative means of increasing P_i transport rates of the COS-7 cells, the human Na^+/Pi cotransporter PiT2 was co-expressed along with the FLIPPi-30m sensor. When cells co-expressing FLIPPi-30m and PiT2 were perfused with P_i, changes in the fluorescence ratio consistent with increased steady-state levels of P_i in the cytosol were observed (Fig. 4d). On rare occasions, a similar response was obtained in cells expressing only FLIPPi-30m (data not shown). The response to the external P_i supply was greater in COS-7 cells than in starved CHO cells, possibly as a consequence of the robust P_i transport activity of PiT2, as well as increased cell viability. To confirm that the changes in emission intensity ratio were a consequence of changes in the cytosolic P_i level, and not of secondary effects induced by external P_i, the response of COS-7 cells was measured in a buffer in which the sodium in Tyrode's saline solution was replaced with choline (since P_i uptake is mediated by Na^+/P_i co-transporters, the absence of a sodium gradient should prevent uptake of P_i). Equilibration of the cells into the Tyrode's choline buffer yielded a lower FRET ratio (perhaps through solution effects on the fluorophore dipoles), but also abolished P_i-dependent changes (Fig. 4e), suggesting that the response of the sensor is indeed specifically due to P_i import by the Na^+/P_i cotransporter. Taken together, these results suggest that in the presence of sufficient transport activity, P_i metabolism may be monitored in a variety of mammalian cell types.

4. Discussion

P_i plays a number of important roles in all cellular compartments. ^{31}P-NMR allows the determination of cellular P_i levels, and can distinguish between different P_i pools in cases where pH differs between compartments [2]. The methodology allows dynamic measurements, but is of insufficient sensitivity for single cell studies. P_i concentrations may be tracked in large compartments such as the plant vacuole, which is more acidic than the cytoplasm [27], but organelles such as the ER, peroxisomes, plastids, and mitochondria either have too small P_i pools and/or a pH near the cytosolic pH value, which makes the signal indistinguishable from the background noise or superimposed on the cytosolic P_i signal, respectively. In addition, a P_i signal from a specific compartment may be NMR invisible because of fast spin–spin relaxation caused by compounds present in the compartment. Variant P_i transporters are present in the inner mitochondrial membrane [30] and in plastids [31], suggesting that both steady-state and dynamic levels of P_i may be quite different for the various sub-cellular compartments.

Therefore, novel methods and reagents are required for the detection of P_i concentrations with sufficient spatial and temporal resolution to address the complex issue of P_i homeostasis. Recently, genetically-encoded FRET sensors have been developed for monitoring calcium, various sugars and amino acids [13,18,32,33]. These sensors make use of a designed allosteric linkage between an analyte-binding recognition element

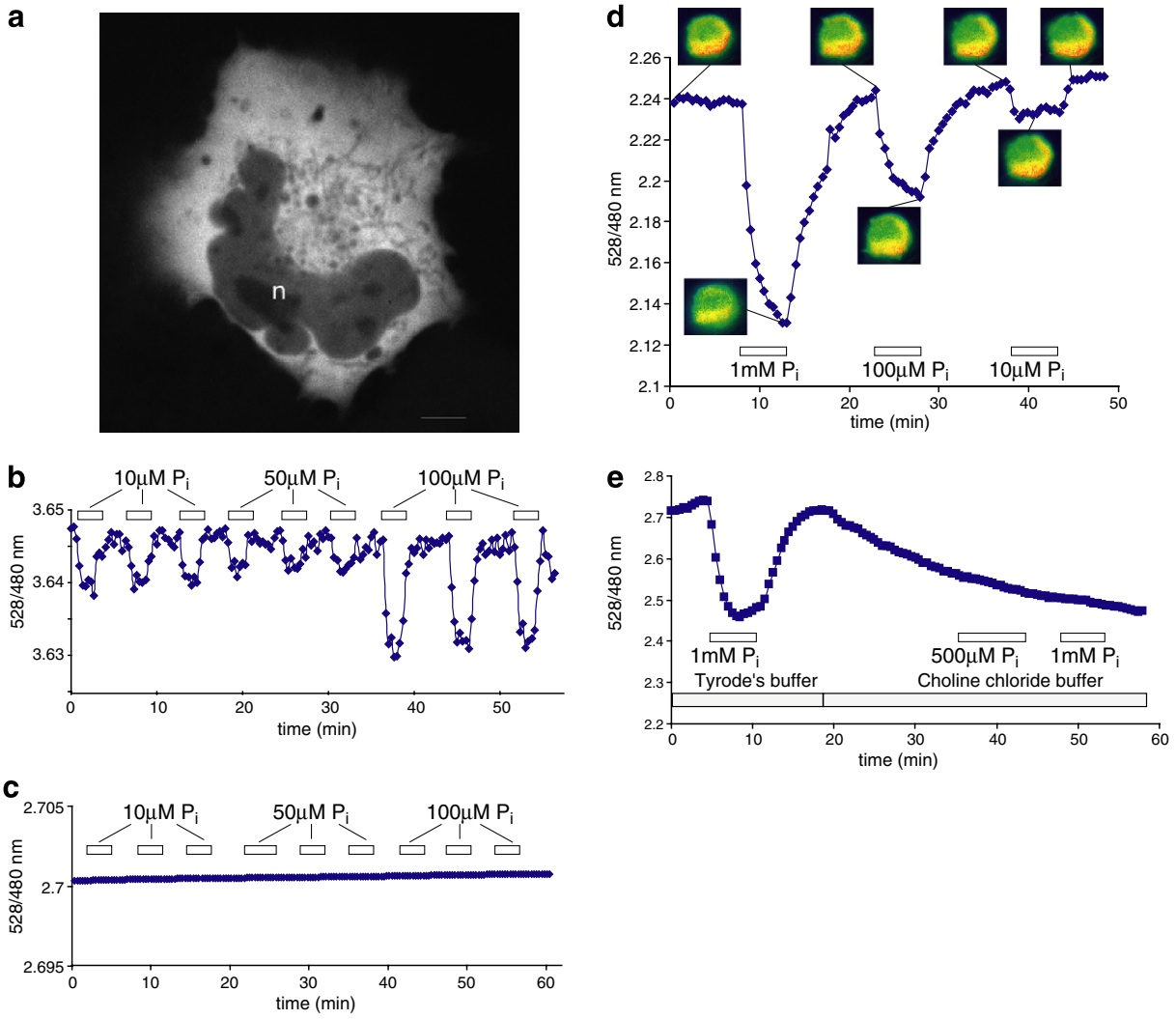

Fig. 4. FRET ratio change in response to P_i perfusion of P_i-starved CHO cells, and COS-7 cells co-expressing a Na^+/Pi cotransporter. (a) Confocal image of a COS-7 cell expressing FLIPPi-30m. Fluorescence is largely excluded from the nucleus (n). The scale bar represents 5 μm. (b) The low-affinity "working" sensor FLIPPi-30m in P_i-starved CHO cells. (c) The high-affinity "control" sensor FLIPPi-5μ is saturated and does not respond to P_i perfusion. (d) The FLIPPi-30m sensor in resting COS-7 cells co-expressing the sodium-dependent phosphate cotransporter PiT2. (e) In sodium-free modified Tyrode's choline buffer, the response of the sensor to P_i is abolished. The boxed numbers indicate the P_i concentration used for perfusion.

(ideally with a significant binding-induced conformational change; calmodulin was employed for the calcium sensor, bacterial periplasmic-binding proteins for the others) and a macroscopic signal-producing reporter element (in this case, FRET-capable cyan and yellow variants of GFP).

Bacterial periplasmic-binding proteins (PBPs) exhibit a conserved domain structure of two (in rare examples, three) α/β lobes connected by β-strand "hinge" elements [34]. A ligand-binding cleft is formed at the interface between the two lobes; upon binding, a hinge-bending motion sequesters the ligand, excluding solvent and presenting functionally-compatible binding site groups from both protein lobes [34,35]. It is this hinge-bending motion that allosterically reorients the reporter fluorophores (in this report, linearly fused to the N- and C-termini of the PBP sequence), giving rise to a change in FRET. Relative fluorophore separation is generally considered to be the dominant feature in resonance energy transfer, reflected in its inverse-sixth power dependence in the Förster equation [36]. Relative fluorophore angular orientation has also been shown to be of great importance [37], and in complex systems such as a chimeric multi-domain protein, these terms are likely to be highly inter-dependent.

The *E. coli* PiBP protein is a type II periplasmic-binding protein [6], with both N- and C-termini on the same protein lobe. A naive first-order approximation of fluorophore position and conformation suggests that the absence of a clear binding-driven lever-arm displacement of the fluorophores relative to one another would produce similar fluorophore relative positional and orientational ensembles in the ligand-free open and ligand-bound closed states, yielding a sensor with a negligible FRET signal change. When the *E. coli* PiBP was converted to a FRET sensor, it did indeed fail to exhibit a significant ligand-dependent FRET change. Hypothesizing that the positioning of protein termini is a weakly selected trait, we pursued a number of other putative P_i-binding proteins as recognition elements in FRET constructs, as a way

to maximize the chance of finding a combination of terminal positions that would enable the construction of a viable sensor. Six additional putative P_i-binding proteins were tested (all predicted to be type II PBPs), and of these, five failed to show a significant P_i-dependent response, suggesting that the first-order model is a powerful discriminator of functional and non-functional sensors. However, a single predicted PiBP of the seven tested (from the thermophilic cyanobacterium *Synechococcus* strain OS-A; three other highly homologous *Synechococcus* proteins failed to signal) produced a sensor with an acceptable signal change. This result, combined with the prior observations that both the type II *E. coli* glutamate/aspartate-binding protein [17] and sensors in which one of the fluorophores has been inserted into the binding protein sequence on the same lobe as the other terminally-fused fluorophore [20] may also produce viable FRET sensors, implies that allosteric propagation more subtle than the lever-arm motion may also give rise to fluorophore reorientation sufficient to produce a FRET change (Fig. 5). To this end, we have performed simple modeling of fluorophore position which suggests that the ligand-driven movement of the second protein lobe of a type II-binding protein may sterically re-position one or both of the fluorophores attached to the terminal lobe (data not shown). Furthermore, it is possible that the binding protein and fluorophores form nascent protein–protein interactions at the site of each chimeric attachment point, through which conformational changes may be allosterically propagated even in the absence of a dramatic re-positioning by the other protein lobe.

The affinity of the *Synechococcus* PiBP proved to be close to that of the *E. coli* PiBP, and the signal change of the initial FRET construct was of similar magnitude to the other PBP-based FRET sensors constructed thus far. Site-directed mutagenesis produced a family of P_i sensors with improved signal change and P_i affinities varying over almost eight orders of magnitude.

This set of P_i sensors should be suitable for monitoring P_i transport and metabolism, such as that previously reported for glucose detection using an analogous FLIPglu sensor in COS-7 and HepG2 cells [14], and for ribose detection using a FLIPrib sensor [15]. FLIPPi sensors (both high-affinity "control" and low-affinity "working" sensors) expressed in the cytosol of non-starved CHO cells failed to show a signal change upon perfusion with P_i up to 10 mM (data not shown). This failure of the sensors to signal may have a number of explanations: the P_i concentration is much lower than previously thought, and the sensors are not seeing their ligand (unlikely, as a sensor with 5 μM affinity shows no response); the P_i concentration is much higher than previously thought, and the sensors are fully-saturated (unlikely, as a sensor with 30 mM affinity shows no response); the P_i concentration is maintained within an interval above the dynamic range of the 5 μM sensor and below that of the 30 mM sensor, i.e. the low millimolar range; or that net P_i influx into the cytosol is small compared to the rates of metabolic conversion and compartmentalization. In an attempt to distinguish between these potential explanations, CHO cells were P_i-starved for 14 h, and the measurement was repeated with the low-affinity sensor. The P_i-starved cells now showed a small but significant signal change upon P_i perfusion; this argues against the maintenance of P_i levels in the low millimolar range, as the P_i levels would have been decreased further below the dynamic range of the sensor.

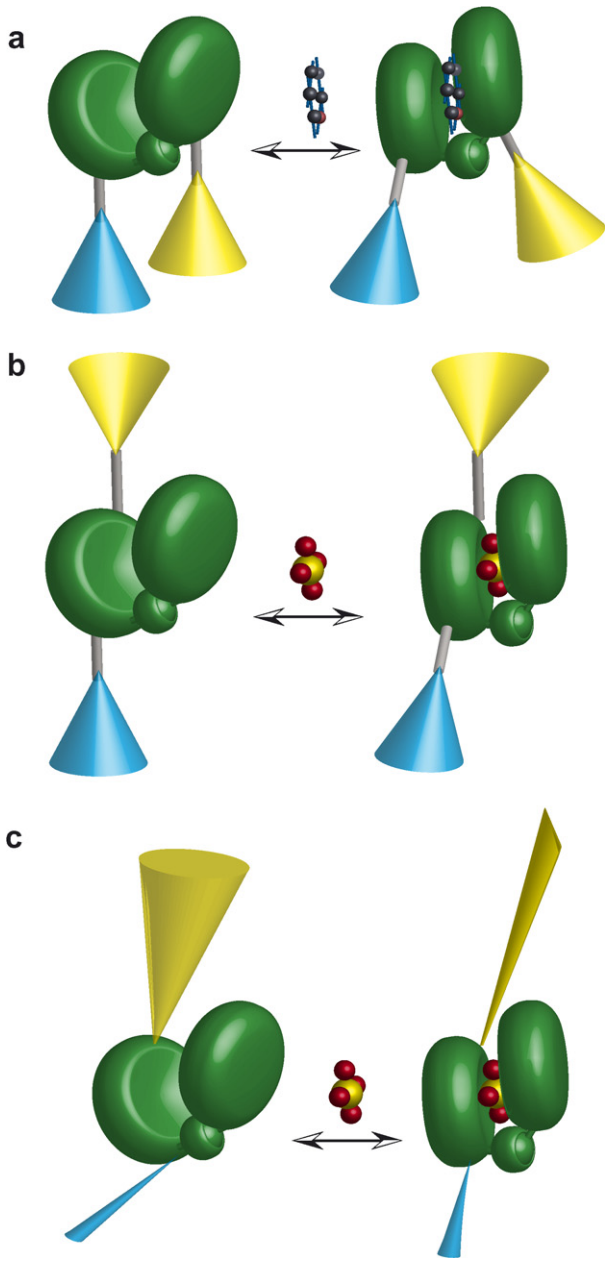

Fig. 5. Cartoon models of FLIPPi sensor function [20]. (a) Model of FLIP sensor developed from type I periplasmic binding proteins (e.g. FLIPglu glucose binding protein [14,15]). Fluorophores (eCFP, cyan; Venus, yellow) attached on two different lobes of a binding protein (consisting of two lobes connected by a hinge, green) via linkers (grey rods). Ligand binding transduces a hinge-binding motion propagated through a lever arm to macroscopically reorient the relative excitation–emission dipole. (b) Model of a FLIP sensor developed from type II PiBPs, in which both fluorophores are attached to the same lobe. Allosteric effects of domain closure propagate into relative dipole reorientation. (c) Shortening or rigidification of a binding protein–fluorophore linker increases the degree of allosteric coupling between ligand binding and fluorophore reorientation. One possible scenario is shown here, in which the closure of the PiBP leads to a restriction in the rotational freedom of eYFP, illustrated as a change in the cone diameter.

Rather, it is most likely that P_i transport rates increased following starvation, and that the level of uptake exceeded the net effect of metabolism and compartmentalization. Hence, P_i perfusion of the P_i-starved cells resulted in a change in the cytosolic P_i concentration.

The P_i-starved CHO cells proved to be rather fragile, making long-term monitoring impossible. As a second demonstration that the response of the sensors is P_i transport-limited, we co-expressed the low-affinity FLIPPi sensor along with the Na^+/Pi transporter PiT2 in COS-7 cells. Much larger FRET changes were then observed, indicating that the introduced P_i transporter contributed more to net P_i influx than the presumed up-regulation of endogenous P_i transporters following P_i starvation. Interestingly, P_i levels in the cytosol of COS-7 cells co-expressing PiT2 promptly decreased when the external P_i supply was removed; it is not known whether this is due to metabolism or to a net efflux of P_i into the bulk medium in response to the strong P_i gradient (or to both).

The currently available FLIPPi sensors should be sufficient to follow P_i metabolism in non-transport-limited cellular environments. Further rounds of protein engineering should produce a sensor with an affinity in the low millimolar range (thus closing the gap between the FLIPPi-200μ and FLIPPi-30m sensors), as well as a sensor with improved signal-to-noise ratio (in vivo FRET changes are invariably lower than those seen in vitro [14,15,17,38], perhaps due to ionic strength, pH, and quenching effects in the cellular milieu). We can at present not exclude that the FLIPPi-30m recognizes other phosphate-containing analytes. Thus, it will be important to compare the results obtained with the sensors in parallel with ^{31}P NMR and other methods.

Production of a sensor for glucose-6-phosphate, combined with the P_i sensor reported here and the previously reported glucose sensor [38], should facilitate monitoring of the principal players in glucose metabolism. A battery of these sensors targeted to the cytosol and the ER should shed light on the complex metabolism and transport events involved in gluconeogenesis and glycolysis [39].

5. Conclusions

A putative PiBP from a thermophilic *Synechococcus* strain was successfully converted into a genetically-encoded P_i sensor. Site-directed mutagenesis facilitated the generation of affinity mutants covering a wide range of physiologically relevant P_i concentrations. So far an extensive mutagenesis has not yielded a suitable mutant (Hong Gu, unpublished). The sensors were used to measure P_i homeostasis in cultured cells in real time. A major advantage of genetically-encoded nanosensors is the ability to target the proteins to subcellular compartments, as demonstrated for the FLIPglu glucose sensor in nuclei [19] and the FLIPE glutamate sensor on the surface of PC12 neuronal cells [17]. The P_i sensors will be useful for a wide range of applications, e.g. to study P_i uptake and translocation, and regulatory mechanisms controlling compartmental P_i homeostasis. The sensors may also be useful tools to study relevant physiological or pathophysiological cellular conditions, e.g., cell motility, by analysis of potential differences between motile and sessile cells or compartmentalized responses in lamellipodia or ruffles. Furthermore, transgenic organisms expressing FLIPPi should allow the visualization of P_i activity directly in organ slices or whole organisms, such as that demonstrated for the calcium FRET indicator cameleon in *Caenorhabditis elegans* neurons [40].

Acknowledgements: We are grateful to Dr. Heard (Institute Pasteur, France) for providing the PiT2 clone. This work was made possible by a grant from HFSP (RGP0041/2004C) to Kristoffer Almdal (Risø, Denmark), I.J., J.K. and W.B.F. H.G. was supported in part by the Danish Research School for Biotechnology FOBI. This work was also partially funded by the Frontiers in Integrative Biology program at NSF (GC036/04/Z3423).

Appendix A. Supplementary data

Supplementary data associated with this article can be found, in the online version, at doi:10.1016/j.febslet.2006.09.048.

References

[1] Collins, J.F., Bai, L. and Ghishan, F.K. (2004) The SLC20 family of proteins: dual functions as sodium-phosphate cotransporters and viral receptors. Pflügers Arch. 447, 647–652.
[2] Vidal, G., Gallis, J.L., Dufour, S. and Canioni, P. (1997) NMR studies of inorganic phosphate compartmentation in the isolated rat liver during acidic perfusion. Arch. Biochem. Biophys. 337, 317–325.
[3] Wang, Z.M., Choudhary, A., Ledvina, P.S. and Quiocho, F.A. (1994) Fine-tuning the specificity of the periplasmic phosphate transport receptor – site-directed mutagenesis, ligand-binding, and crystallographic studies. J. Biol. Chem. 269, 25091–25094.
[4] Medveczky, N. and Rosenberg, H. (1970) Phosphate-binding protein of *Escherichia coli*. Biochim. Biophys. Acta 211, 158.
[5] Brune, M., Hunter, J.L., Corrie, J.E.T. and Webb, M.R. (1994) Direct, real-time measurement of rapid inorganic-phosphate release using a novel fluorescent probe and its application to actomyosin subfragment-1 ATPase. Biochemistry 33, 8262–8271.
[6] Ledvina, P.S., Yao, N.H., Choudhary, A. and Quiocho, F.A. (1996) Negative electrostatic surface potential of protein sites specific for anionic ligands. Proc. Natl. Acad. Sci. USA 93, 6786–6791.
[7] Ledvina, P.S., Tsai, A.L., Wang, Z.M., Koehl, E. and Quiocho, F.A. (1998) Dominant role of local dipolar interactions in phosphate binding to a receptor cleft with an electronegative charge surface: equilibrium, kinetic, and crystallographic studies. Protein Sci. 7, 2550–2559.
[8] Salins, L.L.E., Deo, S.K. and Daunert, S. (2004) Phosphate binding protein as the biorecognition element in a biosensor for phosphate. Sensor. Actuat. B – Chem. 97, 81–89.
[9] Hirshberg, M., Henrick, K., Haire, L.L., Vasisht, N., Brune, M., Corrie, J.E.T. and Webb, M.R. (1998) Crystal structure of phosphate binding protein labeled with a coumarin fluorophore, a probe for inorganic phosphate. Biochemistry 37, 10381–10385.
[10] De Lorimier, R.M. et al. (2002) Construction of a fluorescent biosensor family. Protein Sci. 11, 2655–2675.
[11] Zaccolo, M. (2004) Use of chimeric fluorescent proteins and fluorescence resonance energy transfer to monitor cellular responses. Circ. Res. 94, 866–873.
[12] Lalonde, S., Ehrhardt, D.W. and Frommer, W.B. (2005) Shining light on signaling and metabolic networks by genetically encoded biosensors. Curr. Opin. Plant Biol. 8, 574–581.
[13] Fehr, M., Frommer, W.B. and Lalonde, S. (2002) Visualization of maltose uptake in living yeast cells by fluorescent nanosensors. Proc. Natl. Acad. Sci. USA 99, 9846–9851.
[14] Fehr, M., Lalonde, S., Lager, I., Wolff, M.W. and Frommer, W.B. (2003) In vivo imaging of the dynamics of glucose uptake in the cytosol of COS-7 cells by fluorescent nanosensors. J. Biol. Chem. 278, 19127–19133.
[15] Lager, I., Fehr, M., Frommer, W.B. and Lalonde, S. (2003) Development of a fluorescent nanosensor for ribose. FEBS Lett. 553, 85–89.
[16] Ye, K. and Schultz, J.S. (2003) Genetic engineering of an allosterically based glucose indicator protein for continuous glucose monitoring by fluorescence resonance energy transfer. Anal. Chem. 75, 3451–3459.
[17] Okumoto, S., Looger, L.L., Micheva, K.D., Reimer, R.J., Smith, S.J. and Frommer, W.B. (2005) Detection of glutamate release from neurons by genetically encoded surface-displayed FRET nanosensors. Proc. Natl. Acad. Sci. USA 102, 8740–8745.

[18] Fehr, M. et al. (2005) Development and use of fluorescent nanosensors for metabolite imaging in living cells. Biochem. Soc. Trans. 33, 287–290.
[19] Fehr, M., Lalonde, S., Ehrhardt, D.W. and Frommer, W.B. (2004) Live imaging of glucose homeostasis in nuclei of COS-7 cells. J. Fluoresc. 14, 603–609.
[20] Deuschle, K., Okumoto, S., Fehr, M., Looger, L.L., Kozhukh, L. and Frommer, W.B. (2005) Construction and optimization of a family of genetically encoded metabolite sensors by semirational protein engineering. Protein Sci. 14, 2304–2314.
[21] Nagai, T., Ibata, K., Park, E.S., Kubota, M., Mikoshiba, K. and Miyawaki, A. (2002) A variant of yellow fluorescent protein with fast and efficient maturation for cell-biological applications. Nature Biotechnol. 20, 87–90.
[22] Steunou, A.S. et al. (2006) In situ analysis of nitrogen fixation and metabolic switching in unicellular thermophilic cyanobacteria inhabiting hot spring microbial mats. Proc. Natl. Acad. Sci. USA 103, 2398–2403.
[23] Contreras-Moreira, B. and Bates, P.A. (2002) Domain fishing: a first step in protein comparative modelling. Bioinformatics 18, 1141–1142.
[24] Luecke, H. and Quiocho, F.A. (1990) High specificity of a phosphate transport protein determined by hydrogen-bonds. Nature 347, 402–406.
[25] Desmoulin, F., Cozzone, P.J. and Canioni, P. (1987) Phosphorus-31 nuclear-magnetic-resonance study of phosphorylated metabolites compartmentation, intracellular pH and phosphorylation state during normoxia, hypoxia and ethanol perfusion, in the perfused rat liver. Eur. J. Biochem. 162, 151–159.
[26] Chen, K.Y. (1999) Study of polyphosphate metabolism in intact cells by 31-P nuclear magnetic resonance spectroscopy. Prog. Mol. Subcell. Biol. 23, 1.
[27] Rebeille, F., Bligny, R., Martin, J.B. and Douce, R. (1983) Relationship between the cytoplasm and the vacuole phosphate pool in *Acer pseudoplatanus* cells. Arch. Biochem. Biophys. 225, 143–148.
[28] Pfister, M.F., Hilfiker, H., Forgo, J., Lederer, E., Biber, J. and Murer, H. (1998) Cellular mechanisms involved in the acute adaptation of OK cell Na^+/Pi-cotransport to high- or low-Pi medium. Pflügers Arch. 435, 713–719.
[29] Rodrigues, P. and Heard, J.M. (1999) Modulation of phosphate uptake and amphotropic murine leukemia virus entry by post-translational modifications of PIT-2. J. Virol. 73, 3789–3799.
[30] Krämer, R. (1996) Structural and functional aspects of the phosphate carrier from mitochondria. Kidney Int. 49, 947–952.
[31] Knappe, S., Flügge, U.I. and Fischer, K. (2003) Analysis of the plastidic phosphate translocator gene family in Arabidopsis and identification of new phosphate translocator-homologous transporters, classified by their putative substrate-binding site. Plant Physiol. 131, 1178–1190.
[32] Romoser, V.A., Hinkle, P.M. and Persechini, A. (1997) Detection in living cells of Ca^{2+}-dependent changes in the fluorescence emission of an indicator composed of two green fluorescent protein variants linked by a calmodulin-binding sequence – a new class of fluorescent indicators. J. Biol. Chem. 272, 13270–13274.
[33] Miyawaki, A., Llopis, J., Heim, R., McCaffery, J.M., Adams, J.A., Ikura, M. and Tsien, R.Y. (1997) Fluorescent indicators for Ca^{2+} based on green fluorescent proteins and calmodulin. Nature 388, 882–887.
[34] Fukami-Kobayashi, K., Tateno, Y. and Nishikawa, K. (1999) Domain dislocation: a change of core structure in periplasmic binding proteins in their evolutionary history. J. Mol. Biol. 286, 279–290.
[35] Shilton, B.H., Flocco, M.M., Nilsson, M. and Mowbray, S.L. (1996) Conformational changes of three periplasmic receptors for bacterial chemotaxis and transport: the maltose-, glucose/galactose- and ribose-binding proteins. J. Mol. Biol. 264, 350–363.
[36] Förster, T. (1948) Intermolecular energy migration and fluorescence. Ann. Phys. 2, 55–75.
[37] Van Der Meer, B.W., Cooker, G.I. and Chen, S.Y.S. (1994) Resonance Energy Transfer: Theory and Data, VCH Publishers, New York.
[38] Fehr, M., Takanaga, H., Ehrhardt, D.W. and Frommer, W.B. (2005) Evidence for high-capacity bidirectional glucose transport across the endoplasmic reticulum membrane by genetically encoded fluorescence resonance energy transfer nanosensors. Mol. Cell. Biol. 25, 11102–11112.
[39] Arion, W.J. and Canfield, W.K. (1993) Glucose-6-phosphatase and type 1 glycogen storage disease: some critical considerations. Eur. J. Pediatr. 152 (Suppl. 1), S7–S13.
[40] Kerr, R., Lev-Ram, V., Baird, G., Vincent, P., Tsien, R.Y. and Schafer, W.R. (2000) Optical imaging of calcium transients in neurons and pharyngeal muscle of *C. elegans*. Neuron 26, 583–594.
[41] Kunkel, T.A., Roberts, J.D. and Zakour, R.A. (1987) Rapid and efficient site-specific mutagenesis without phenotypic selection. Meth. Enzymol. 154, 367–382.